ADVANCED MATERIALS

Absorption and Emission in Quaterthienyl Thin Films**

By *Hao Sun*, *Zhen Zhao*, *Frank C. Spano*,* *David Beljonne*, *Jérôme Cornil*, *Zhigang Shuai*, and *Jean-Luc Brédas*

A large number of experimental and theoretical works have been devoted to thin films, aggregates, and crystals of thiophene oligomers αT*n* (with *n* the number of thiophene rings), aiming particularly at unraveling the role of intermolecular interactions on the electronic structure and optical properties of these materials.[1–11] These studies are motivated by the fact that such materials can be fashioned into field-effect transistors and light-emitting diodes.[1] However, questions remain regarding the fundamental photophysical properties of αT*n* assemblies. For example, there is no consensus regarding the magnitude of the Davydov splitting (DS).[2–7] In αT6 crystals, values ranging from 120 cm^{-1}[2] to 10 000 cm^{-1}[3] have been reported. Furthermore, αT*n* thin films and aggregates show an unusual intensity distribution in the vibronic emission bands, with a 0–0 intensity that does not fit the usual intensity distribution for a Franck–Condon (FC) progression.[2,8–11]

In this work, we present a theoretical model which accounts for the salient features in the absorption and emission spectra of αT4 thin films. The same model was recently used to account for the very similar photophysical properties of distyrylbenzene aggregates.[12–14] We find that for incoming light with wave vector $\boldsymbol{k}$ normal to the herringbone (*ab*) plane, the DS is on the order of or larger than 1 eV. Furthermore, the (broad) absorption features observed at ≈800 cm^{-1} and ≈2900 cm^{-1} above the band origin[2,4,9] are due to vibrationally dressed excitons, located far below the strongly allowed upper Davydov component. The latter is due to an exciton almost entirely uncoupled from vibrations. In defect-free crystals, the weakly allowed lower Davydov component is the origin of *b*-polarized 0–0 emission. The 0–0 emission is coherently enhanced and can even become superradiant,[11–14] but is easily quenched by basal plane structural defects.[12] In stark contrast, the mainly *ac*-polarized phonon replicas are not coherently enhanced and are virtually insensitive to basal plane defects.[12]

Aggregate Model: The packing within an αT4 thin film is assumed to conform to that within an αT4 crystal;[2] molecular clusters of increasing size are built from the low-temperature form.[15] A view down the long molecular axes in a 5×5 aggregate is provided in the structural items inset in Figure 1. We consider aggregates cut from a single herringbone (*ab*) plane since intermolecular interactions between adjacent molecules in different planes is much weaker than that between adjacent molecules within the same plane.[16]

In our model all molecules are treated as electronic two-state systems (ground, 1^1A_g and excited, 1^1B_u) coupled to a single *effective* intramolecular vibrational mode of frequency ω_0. The intramolecular vibration is related to the symmetric ring breathing mode at approximately 1470 cm^{-1} in αT4.[1] There are also several low-frequency modes coupled to the $1^1A_g \rightarrow 1^1B_u$ transition which provide fine structure to the absorption spectrum. Such structure is not accounted for in the present model. The nuclear potential wells for the 1470 cm^{-1} mode are assumed to be harmonic in both the 1^1A_g and 1^1B_u states, and of identical curvature, but displaced relative to each other. The displacement gives rise to a nonzero Huang–Rhys factor, λ^2, which is approximately unity. Upon aggregation, the 0–0 transition frequency, $\omega_{0\text{–}0}$, undergoes a gas-to-crystal shift, $D_{\boldsymbol{n}}$ at site $\boldsymbol{n}$. In what follows, $D_{\boldsymbol{n}} = D$ is taken to be an adjustable parameter independent of $\boldsymbol{n}$ for defect-free aggregates.

The intermolecular interactions, $J_{\boldsymbol{mn}}$, between a molecule at $\boldsymbol{m}$ and one at $\boldsymbol{n}$, are evaluated on the basis of the atomic transition densities for the isolated molecules[17]; these are calculated at the INDO[18]/MRD-CI level using the X-ray geometric structure;[15] the Mataga–Nishimoto[19] potential was adopted to depict both intrachain and interchain electron–electron interactions. We stress that "supermolecular" calculations including charge-transfer excitations and higher lying excitations lead to very similar results.[20]

In a one-exciton representation, the aggregate Hamiltonian reads:[12–14]

$$H = \omega_0 \sum_{\boldsymbol{n}} b_{\boldsymbol{n}}^{\dagger} b_{\boldsymbol{n}} + \omega_0 \lambda \sum_{\boldsymbol{n}} (b_{\boldsymbol{n}}^{\dagger} + b_{\boldsymbol{n}}) \; |\boldsymbol{n}\rangle \langle \boldsymbol{n}| + \sum_{\boldsymbol{m}} \sum_{\boldsymbol{n}} (\delta_{\boldsymbol{mn}} D_{\boldsymbol{n}} + J_{\boldsymbol{mn}}) \; |\boldsymbol{m}\rangle \langle \boldsymbol{n}| + \omega_{0\text{–}0} + \lambda^2 \omega_0 \qquad (1)$$

where $\hbar = 1$ is taken, and zero energy corresponds to the state with no electronic or vibrational excitations. $b_{\mathbf{n}}^{\dagger}(b_{\mathbf{n}})$ is the creation (destruction) operator for the harmonic oscillator representing the ground potential (1^1A_g) vibration on molecule $\boldsymbol{n}$. In the pure electronic state, $|\mathbf{n}\rangle$, the molecule at $\boldsymbol{n}$ is electronically excited to the 1^1B_u state while all others remain in their 1^1A_g ground states.

The eigenstates, $|\Psi^{(j)}\rangle$, and associated energies, $\varepsilon^{(j)}$ of H are evaluated numerically using the two-particle approximation as described by Spano,[12] with a maximum of four vibrational

[*] Prof. F. C. Spano, H. Sun, Z. Zhao
Department of Chemistry, Temple University
Philadelphia, PA 19122 (USA)
E-mail: spano@astro.temple.edu
Dr. D. Beljonne, Dr. J. Cornil, Dr. Z. Shuai, Prof. J.-L. Brédas
Chemistry of Novel Materials, University of Mons-Hainaut,
Place du Parc 20, B-7000 Mons (Belgium)
Dr. D. Beljonne, Dr. J. Cornil, Prof. J.- L. Brédas
Department of Chemistry, The University of Arizona
Tucson, AZ 85721-0041 (USA)
Dr. Z. Shuai
Center for Molecular Science, Institute of Chemistry
The Chinese Academy of Sciences
Beijing 100080 (P.R. China)

[**] The Temple group is supported by the National Science Foundation (grant DMR-0071802). The work at Arizona is partly supported by the National Science Foundation (grant CHE-0078819), the Office of Naval Research, and the IBM Shared University Research Program. The work in Mons is partly supported by the Belgian Federal Services for Scientific, Technical, and Cultural Affairs (InterUniversity Attraction Pole 5/3) and the Belgian National Science Foundation (FNRS). David Beljonne and Jérôme Cornil are Research Associates from FNRS. ZS is supported by the NSFC Grant No. 90203015 and the "973 program" Grant No. 2002CB613406.

  DOI: 10.1002/adma.200304770

quanta per aggregate. From these, the dimensionless polarized absorption spectrum, $\alpha_\delta(\omega)$, *per molecule* takes the form:[12]

$$\alpha_\delta(\omega) = (NW_a(0)\mu^2)^{-1} \sum_j |< G|\hat{M}_\delta|\Psi^{(j)}>|^2 W_a(\omega - \varepsilon^{(j)}) \quad (2)$$

where $\delta = a$, b, or c, N is the number of molecules and $\mu^2 = \mu_\parallel^2 + \mu_\perp^2$. Here, $\mu_\parallel$ and $\mu_\perp$ are the long and short axis component of the molecular $1^1A_g \rightarrow 1^1B_u$ transition dipole moment (tdm), respectively (see Figure 1). The *aggregate* tdm operator, $\hat{M}$,[12] allows one-photon excitation from the aggregate

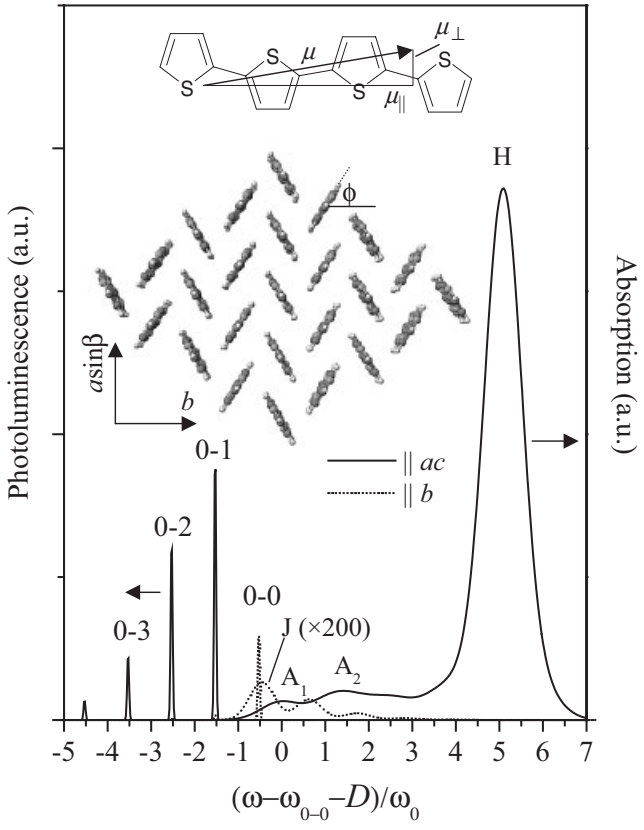

Fig. 1. Calculated absorption and emission spectra using Equations 2 and 3 respectively, for the 5×5 aggregate shown in the inset, as viewed down the long molecular axis ($a = 6.088$ Å, $b = 7.858$ Å, $\beta = 91{,}81°$, and $\phi = 61°$) [15]. The line shape functions used in the absorption and emission spectra are, $W_a(\omega) = \exp[-(\omega/0.65\omega_0)^2]$ and $W_e(\omega = \exp[-(\omega/0.05\omega_0)^2]$, respectively. In addition, $\lambda^2 = 1$ and $\omega_0 = 1470$ cm^{-1}. Inset also shows the molecular structure of αT4 with the $1^1A_g \rightarrow 1^1B_u$ tdm. Our MRD/CI calculations give $\mu_\perp = 0.05\ \mu_\parallel$.

ground state, $|G\rangle$, to the jth exciton, $|\Psi^{(j)}\rangle$ Finally, $W_a(\omega)$ is the line shape function representing inhomogeneous broadening.

The emission spectrum is similarly divided into components polarized along a, b, and c with the δth component given by, [12]

$$S_\delta(\omega) = \sum_{\nu_t t=0,1,2,\ldots} I_\delta(\nu_t)(1 - \nu_t\omega_0/\omega_{em})^3 \times W_e(\omega - \omega_{em} + \nu_t\omega_0)/W_e(0) \quad (3)$$

Here, ω_{em} is the frequency of the emitting state, $W_e(\omega)$ is the emission line shape function and $I_\delta(\nu_t)$ is the dimensionless 0–ν_t line strength for δ-polarized emission, given by:

$$I_\delta(\nu_t) = \frac{1}{\mu^2} \sum_{\{\nu_n\}}{}' |< \Psi^{(em)}|\hat{M}_\delta \prod_n |g_n, \nu_n>|^2 \quad (4)$$

where $\Pi_n |g_n,\nu_n>$ is a terminal state in the emission event in which the molecule at n is in the electronic ground state with ν_n vibrational quanta in the 1^1A_g potential. The prime on the summation in Equation 4 indicates the constraint $\sum_n \nu_n = \nu_t$.

The calculated absorption and emission spectra for a 5×5 aggregate are displayed in Figure 1. The weak b-polarized absorption origin (J), is the lowest Davydov component made optically allowed by the small deviation of the tdm from the long molecular axis (see Fig. 1, inset structures).[3,11,12–14] The ac-polarized peaks, A_1 and A_2, are blue-shifted by approximately 800 and 2900 cm^{-1}, respectively, from the origin, while the main absorption peak, H, which constitutes the upper Davydov component, is blue-shifted by almost 1 eV relative to the origin. Figure 2 shows that the peak positions of J, A_1, and A_2 are virtually size independent,[12,14] while the H-band continues to blue-shift and saturates after a few thousand molecules. Two potentials have been used in Figure 2: the standard Mataga–Nishimoto potential as implemented by Zerner in the ZINDO package (which evolves as $1.2/r$ at long distance) and a modified potential providing the expected $1/r$ dependence at large r. In both cases the resulting 1.6–1.9 eV DS extrapolated for an infinite cluster should be regarded as an

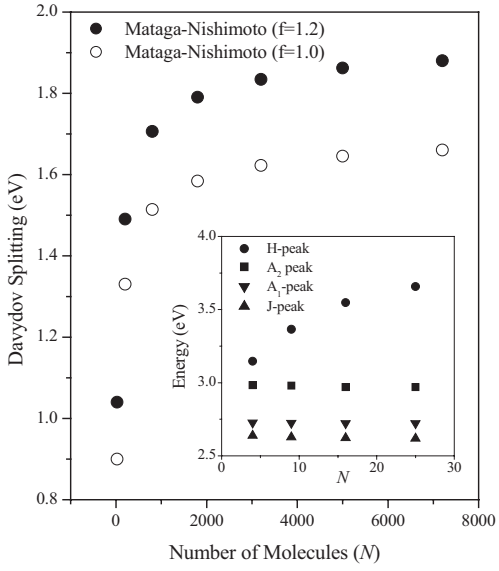

Fig. 2. Davydov splitting for αT4 aggregates as a function of increasing size starting at $N = 25$. To treat large aggregates the upper Davydov component was evaluated from the purely electronic Hamiltonian (i.e., the third term in Equation 1) and increased by $\lambda^2\omega_0 \approx 0.18$ eV appropriate for an unrelaxed or free exciton [12]. The N-independent lower Davydov component evaluated for $N = 25$ using the full Hamiltonian in Equation 1 was used in evaluating the DS for all sizes. Two potentials were used: the standard Mataga–Nishimoto potential and a modified potential providing the correct distance dependence at large r (see Mataga et al. [19] and text). Inset shows the energies of the J, A_1, A_2, and H peaks as a function of N based on the full Hamiltonian in Equation 1.

ADVANCED MATERIALS

upper estimate since the simulations neglect dielectric screening. The effects of screening may be crudely included by dividing the DS by the optical dielectric constant, $\varepsilon_\infty \approx 2$.

The evolution with cluster size of the J, A_1, A_2, and H peaks is strongly influenced by the degree of vibrational dressing of the associated exciton states.[12–14] Peak H is due to a quasi-free exciton which is only weakly coupled to the nuclear motions. The magnitude of the nuclear shift relative to the 1^1A_g minimum for all molecules including the electronically excited one is much smaller than $|\lambda|$. By contrast, the much weaker J, A_1, and A_2 peaks are due to vibrationally relaxed excitons in which the nuclear shift at the site of the electronically excited molecule is close to $|\lambda|$, with smaller but non-negligible shifts on neighboring molecules.[14] Whereas A_1 and J each arise primarily from a single excitonic transition, A_2 arises from a cluser of 4–5 excitonic transitions that are very close in energy. The phonon "cloud" that surrounds all of the low-energy excitons increases their effective mass, leading to low dispersion and size insensitivity (see Fig. 2). A more detailed analysis[14] shows that as the exciton bandwidth increases, the J–A_1 spectral separation increases, eventually converging to ω_0. In this limit A_1 becomes a false origin, arising from the J-band exciton coupled to a single asymmetric phonon, made optically allowed by an intermolecular version of Herzberg–Teller coupling.

The calculated emission spectrum in Figure 1 includes a *b*-polarized 0–0 peak, derived entirely from the off-axis component of the tdm ($\mu_\perp$), and primarily *ac*-polarized replica intensities, derived mainly from $\mu_\parallel$. As shown in the literature[12–14], the 0–0 peak intensity, $I_b(\nu_t = 0)$, increases linearly with N (or, more generally, with the exciton coherence number, N_{coh}) leading to a threshold-activated superradiance, $\gamma_{agg} = (N_{coh}/N_{th})\gamma_{mol}$[13,14] where $\gamma_{agg}(\gamma_{mol})$ is the aggregate (single-molecule) radiative decay rate. $N_{th} = \mu^2/(\mu_\perp^2 F \cos^2 \Phi)$ is the superradiant threshold number. Here F is a generalized FC factor[14] and ϕ is the setting angle (see Fig. 1). For αT4, we calculate $N_{th} \approx 2 \times 10^3$. By stark contrast, the replica intensities diminish with N (or N_{coh}) eventually stabilizing in the large N limit to values orders of magnitude smaller than the origin intensity.[14] Thus, even though the 0–0 line is of modest intensity in the 5×5 aggregate of Figure 1, it will dominate the spectrum for aggregates with $N > 75$. The contrasting (coherence) size dependencies of the 0–0 intensity and the replica intensities makes the 0–0/0–1 intensity ratio extremely sensitive to disorder. In the next section, we describe how the shape of the emission spectrum is affected by the presence of structural defects in αT4 thin films.

Comparison to Experiment: The absorption and photoluminescence (PL) spectra for αT4 thin films measured by Hopmeier et al.[9] are shown in Figure 3. The 2 nm thick films grown on highly oriented pyrolytic graphite (HOPG) consist of highly ordered αT4 microcrystallites, as reflected by the narrow spectral lines, while the 50 nm thick films deposited on glass contain a large number of structural defects, and display considerable line broadening. The highest energy peak in the αT4/HOPG emission spectrum corresponds to 0–0 emission from the lower exciton band. Hopmeier et al.[9] also showed that, in αT4/glass, the emission spectrum evolves with time; an excitonic component identical to that found in αT4/HOPG vanishes after about 200 ps, leaving behind a red-shifted defect spectrum (shown at 700 psec in Fig. 3). Note that the 0–0 peak in the defect spectrum is considerably attenuated relative to the 0–1 peak. An unusually low 0-0 intensity was originally noted by Gebauer and co-workers for αT4 deposited on Ag(111).[2,9] As pointed out by Kouki et al.[2] and Hopmeier et al.,[9] self-absorption *alone* cannot be responsible due to the very low optical density of the thin films.

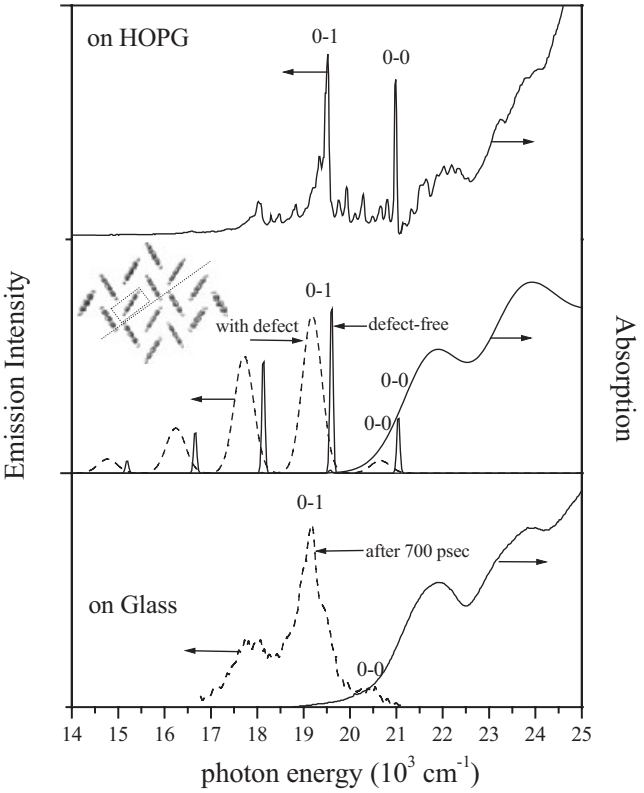

Fig. 3. Experimental absorption and emission spectra for αT4 on HOPG and glass substrates from the literature [9]. The middle panel shows theoretical spectra: the absorption spectrum for a 5×5 aggregate using Equation 2 with $W_a(\omega) = \exp[-(\omega/0.65\omega_0)^2]$, and corresponding emission spectrum. Also shown is the emission spectrum for a defected aggregate consisting of a stacking fault and including a point defect (see text), as shown in the inset. The calculated emission spectra are based on the line shape function $W_a(\omega) = \exp[-(\omega/\sigma_0)^2]$ with $\sigma = 0.05\omega_0$ and $0.2\,\omega_0$ for the defect-free and defected aggregate, respectively. Furthermore, in the defected aggregate all J_{mn} were re-evaluated and the value of D_n was set to $D - 470$ cm^{-1} for the 8 molecules along the fault. Finally, D was adjusted so that the calculated and measured 0–0 emission peaks are aligned.

The theoretical absorption and emission spectra for a defect-free 5×5 aggregate are also shown in Figure 3. Since our model includes only the strongly coupled αT4 vibrational mode at 1470 cm^{-1}, the fine structure in the αT4/HOPG spectra could not be reproduced. However, the overall shape of the simulated absorption spectrum is in remarkable agreement with experiment, namely the calculated A_1 and A_2 peak positions and relative intensities are fully consistent with the experimental data when the line shape function, W_a in Equa-

tion 2 is taken to be gaussian with a half width half maximum (HWHM) = 800 cm^{-1}. The calculations also correctly yield the spectral positions of the main emission peaks in αT4/HOPG.

The experimental finding that disorder inherent in the αT4/glass spectrum reduces the relative intensity of the 0–0 emission line is confirmed by the results of the theoretical simulations including structural disorder. The red-shifted emission spectrum (at 700 ps or steady state) in αT4/glass relative to αT4/HOPG is most likely due to defect emission, as suggested by Hopmeier et al.[9] However, the strongly attenuated 0–0 peak does not conform to the usual Poisson distribution for the vibronic line intensities, based on a displaced harmonic oscillator model for the FC overlap factors. It was shown by Spano[12] that the 0–0 line is far more sensitive to basal plane structural defects than are the replicas. As an example, the stacking fault shown in the inset of Figure 3 annihilates the 0–0 emission due to a destructive interference between emission from molecules on one side of the fault with those on the other side, while leaving the replica intensities relatively unaffected. Interrupting the perfect cancellation adds intensity to the 0–0 line. As shown in Figure 3, this can be accomplished by adding a point defect, which consists of rotating the outlined molecule in Figure 3 about its long axis by 180°. The theory further predicts that the 0–0 line is polarized within the herringbone plane, in contrast to the replicas which are polarized primarily in the *ac* plane. A polarization difference between the 0–0 line and the replicas has been observed in αT4 nanoaggregates by Oelkrug et al.[10] and αT4 and αT6 single crystals by Muccini et al.[4]

Analysis of the wave functions of the excitons responsible for the J, A_1, and A_2 absorption peaks show that they are vibrationally relaxed, low-dispersion (polaronic) excitons, whereas the H peak is due to a highly dispersive nearly free exciton. Thus, the peak positions of J, A_1 and A_2 are practically *N*-independent, while H converges slowly with *N* to about 1.6–1.9 eV/ε_∞ relative to J, depending on the potential adopted. Our results clearly show that when $\boldsymbol{k}$ is normal to the herringbone plane the DS in αT4 aggregates is quite large, on the order of 1 eV, in agreement with the experimental data by Kouki et al[3] and Egelhaaf et al.[10]

The DS attains large values even for the small aggregates in Figure 2, whose dimensions (< 30 nm on an edge) are much smaller than an optical wavelength. For these aggregate sizes there is little or no orientational dispersion,[21] i.e., the DS is independent of the wave vector direction. In the crystal limit, we expect that as long as the wave vector $\boldsymbol{k}$ remains normal to the herringbone (*ab*) plane the DS will remain in the 1.6–1.9 eV/ε_∞ range. However, when $\boldsymbol{k}$ is not normal to the *ab* plane (for example, $\boldsymbol{k} \| \boldsymbol{b}$) the resulting phase variation across the *ab* plane reduces the DS. The orientational dependence of the DS in the crystal limit is due to the long-range behavior of the *instantaneous* interaction sums which determine the exciton dispersion. The interaction sums can be partitioned as $J(\boldsymbol{k}) + 4\pi m(\boldsymbol{\mu}\cdot\hat{\boldsymbol{k}})^2/\varepsilon_\infty \nu_0$, where *m* is the number of molecules per unit cell of volume ν_0, and $\hat{\boldsymbol{k}}$ is a unit vector along $\boldsymbol{k}$.[21] Hence, in the long wavelength limit the energy of the longitudinal exciton ($\boldsymbol{\mu}\cdot\hat{\boldsymbol{k}} = \mu$) exceeds that of the transverse exciton ($\boldsymbol{\mu}\cdot\hat{\boldsymbol{k}} = 0$) by $4\pi m(\boldsymbol{\mu}\cdot\hat{\boldsymbol{k}})^2/\varepsilon_\infty \nu_0$ which is ≈ 0.8 eV for αT6.[7] An orientationally dependent DS has recently been measured in αT6 crystals[7] as well as highly ordered sexiphenyl films,[23] in both cases slightly exceeding 1 eV when $\boldsymbol{k}$ is close to parallel with the long molecular axis.

A direct measurement of the strong H-peak in the crystal limit is difficult in transmission experiments because of the large extinction coefficient. The more readily obtained reflection spectrum can be understood within the framework of polariton theory[22] which predicts a stop band. When $\boldsymbol{k}$ is normal to the *ab* plane (and the electric field is polarized in the *ac* plane) the stop band is narrow and bounded on the high energy side by the longitudinal exciton energy. The (coulombic) exciton energy calculated here is close to the longitudinal exciton energy because $\boldsymbol{k}$ is almost parallel to $\boldsymbol{\mu}$. Hence, our results predict a narrow stop band at approximately 1.6–1.9 eV/ε_∞ above the band origin in αT*n* crystals. Recently, Weiser and Moller[24] measured a strong increase in reflectivity approximately 1.1 eV above the band origin in αT6 crystals in satisfactory agreement with our calculations.

We stress that the calculated DS value is much larger than that reported previously by some authors;[4,5] the model used here is, however, more relevant for the description of the optical properties of the crystal, since all important interactions were included[6] and the size of the aggregates was sufficiently large. The smaller estimates of 2900 cm^{-1} for αT4 (and 2600 cm^{-1} in αT6) [4,5] from polarized absorption measurements on single crystals (with $\boldsymbol{k}$ normal to the herringbone plane)[25] are likely due to mistaking the peak A_2 for the upper Davydov component, a point originally raised by Petelenz and Andrzejak.[6] Recent experiments of Loi et. al[7] interpret peak A_2 as a charge transfer transition, in conflict with our Frenkel exciton interpretation. Moller et al.[26] also argue against a charge transfer origin based on an analysis of their electro-absorption measurements.

In a defect-free film, emission proceeds from the lowest energy exciton. The 0–0 emission is proportional to the exciton coherence volume and hence is a measure of crystalline quality. Recently, Meinardi et al.[11] showed that the 0–0 line is enhanced (relative to the replica intensities) in αT4 films with a greater degree of crystalline order. Longer lived and red-shifted defect emission dominates in samples grown on glass, most likely due to a much higher concentration of structural defects. Here, we analyzed just one of many possible defects; a stacking fault, well known for crystal anthracene,[27] with an included point defect. This defect combination dramatically reduces the 0–0/0–1 intensity ratio. Generally, this ratio decreases in response to any reduction in the exciton coherence length. For example, adding randomly distributed site disorder will also diminish the 0–0/0–1 ratio. The effects of other defects such as small angle grain boundaries and nonbasal edge dislocations are currently under investigation.

Received: December 17, 2002
Final version: March 2, 2003

ADVANCED MATERIALS

[1] C. Ziegler, *Handbook of Organic Conductive Molecules and Polymers*, (Ed: H. Nalwa), Vol. 3, Wiley, Chichester **1997**, Ch. 13.
[2] W. Gebauer, M. Sokolowski, E. Umbach, *Chem. Phys.* **1998**, *227*, 33.
[3] F. Kouki, P. Spearman, P. Valet, G. Horowitz, F. Garnier, *J. Chem. Phys.* **2000**, *113*, 385.
[4] M. Muccini, M. Schneider, C. Taliani, M. Sokolowski, E. Umbach, D. Beljonne, J. Cornil, J. L. Bredas, *Phys. Rev. B* **2000**, *62*, 6296.
[5] M. Muccini, E. Lunedei, C. Taliani, D. Beljonne, J. Cornil, J. L. Bredas, *J. Chem. Phys.* **1998**, *109*, 10 513.
[6] P. Petelenz, M. Andrzejak, *Chem. Phys. Lett.* **2001**, *343*, 139.
[7] M. A. Loi, C. Martin, H. R. Chandrasekhar, M. Chandrasekhar, W. Graupner, F. Garnier, A. Mura, G. Bongiovanni, *Phys. Rev. B* **2002**, *66*, 113 102.
[8] W. Gebauer, M. Bassler, R. Fink, M. Sokolowski, E. Umbach, *Chem. Phys. Lett.* **1997**, *266*, 177.
[9] M. Hopmeier, W. Gebauer, M. Oestreich, M. Sokolowski, E. Umbach, R. F. Mahrt, *Chem. Phys. Lett.* **1999**, *314*, 9.
[10] D. Oelkrug, H.-J. Egelhaaf, J. Gierschner, A. Tompert, *Synth. Met.* **1996**, *76*, 249.
[11] F. Meinardi, M. Cerminara, A. Sassella, A. Borghesi, P. Spearman, G. Bongiavanni, A. Mura, R. Tubino, *Phys. Rev. Lett.* **2002**, *89*, 157 403.
[12] F. C. Spano, *J. Chem. Phys.* **2002**, *116*, 5877.
[13] F. C. Spano, *Chem. Phys. Lett.* **2000**, *331*, 7.
[14] F. C. Spano, *J. Chem. Phys.* **2003**, *118*, 981.
[15] Monoclinic, space group $P2_1/c$, see T. Siegrist, C. Kloc, R. A. Laudise, H. E. Katz, R. C. Haddon, *Adv. Mater.* **1998**, *10*, 379.
[16] J. Cornil, D. Beljonne, J.-P. Calbert, J.-L. Brédas, *Adv. Mater.* **2001**, *13*, 1053.
[17] C. Ecoffet, D. Markovitsi, P. Millié, J. P. Lemaistre, *Chem. Phys.* **1993**, *177*, 629.
[18] J. Ridley, M. Zerner, *Theoret. Chim. Acta* **1998**, *32*, 111.
[19] N. Mataga, K. Nishimoto, *Z. Phys. Chem.* **1957**, *13*, 140. The potential between atomic sites A and B is:

$$\gamma_{AB} = \frac{f}{\frac{2f}{\gamma_{AA}+\gamma_{BB}}+r_{AB}} \quad (5)$$

where $f = 1.2$. r_{AB} is the intersite distance, and γ_{AA} and γ_{BB} are the on-site repulsion terms.
[20] D. Beljonne, F. C. Spano, unpublished.
[21] L. B. Clark, M. R. Philpott, *J. Chem. Phys.* **1970**, *53*, 3790.
[22] M. R. Philpott, *Advances in Chemical Physics* (Eds: I. Prigogine, S. A. Rice), Vol. 23, Wiley, New York **1973**.
[23] E. Zojer, N. Koch, P. Puschnig, F. Meghdadi, A. Niko, R. Resel, C. Ambrosch-Draxl, M. Knupfer, J. Fink, J. L. Bredas, G. Liesing, *Phys. Rev. B* **2000**, *61* 16 538.
[24] G. Weiser, S. Moller, *Phys. Rev. B* **2002**, *65*, 45 203.
[25] Note that the herringbone plane for αT6 in Refs. 4 and 5 is the *bc* plane.
[26] S. Moller, G. Weiser, F. Garnier, *Phys. Rev. B* **2000**, *61*, 15 749.
[27] E. A. Silinsh, *Organic Molecular Crystals, Their Electronic States*, Springer, Berlin **1980**.

Single-Crystalline Scroll-Type Nanotube Arrays of Copper Hydroxide Synthesized at Room Temperature**

By *Weixin Zhang*, *Xiaogang Wen*, *Shihe Yang*,* *Yolande Berta*, and *Zhong Lin Wang**

Soon after the discovery of carbon nanotubes,[1] inorganic analogues of the cage structures such as MQ_2 (M = Mo, W; Q = S, Se) were also synthesized.[2] Subsequently, more nested fullerene-like structures of inorganic compounds were fabricated, including BN and V_2O_5.[3] A common feature of the cage-forming materials is their anisotropic 2D layered structures, which tend to bend and eliminate dangling bonds by the intra-layer linkage.

Many methods for the synthesis of inorganic nanotubes have been based on high-temperature processes. These include chemical vapor transport,[4] sol–gel process,[5] arc-discharge,[6] solvothermal treatment,[7] and oxide nanowhisker growth.[8] Low-temperature routes such as templated synthesis have also been attempted,[9,10] but it has proved difficult to form single-crystalline nanotubes.[11] Gedanken et al. have synthesized scroll-like cylindrical GaOOH[12] and nested fullerene-like nanoparticles of Tl_2O and MoS_2 using sonochemical and sonoelectrochemical methods.[13] This soft technique relies on elevated temperatures and pressures at localized spots. Recently, relatively mild conditions of chemical precipitation were adopted for the synthesis of tube-like structures of $Mg(OH)_2$ and NiS.[14]

$Cu(OH)_2$ has a layered structure with inter-layer hydrogen bonds instead of van der Waals interactions occurring in most of the 2D compounds mentioned above. It is tempting to see whether and how nanoscale tubes could be formed from such a layered structure separated by hydrogen bonds. $Cu(OH)_2$ can be conveniently synthesized in solutions of copper(II). Matijević and co-workers have studied the relationship between the morphologies of homogeneously precipitated $Cu(OH)_2$ and the solution compositions.[15,16] The treatment of high-purity copper ribbon in a solution of ammonia and acetone at 277 K for 3 weeks has allowed single crystals of $Cu(OH)_2$ to be grown by Oswald et al.[17] All the crystals were of similar dimensions with tiny hollows or cavities on the surfaces. In this communication, we report the successful growth of a novel scroll-type nanotube structure of $Cu(OH)_2$ arrayed on a copper foil at ambient temperature and pressure. The synthesis was accomplished by surface oxidation of the copper foil in an alkaline aqueous solution with $(NH_4)_2S_2O_8$.

The X-ray diffraction (XRD) pattern of the as-prepared product on copper foil (Fig. 1) is attributable to the orthorhombic $Cu(OH)_2$ phase (space group: $Cmc2_1$) according to the recent refinement of Oswald et al.[17,18] All the diffraction peaks of Figure 1, except those marked with an asterisk, arising from the copper substrate, can be indexed to this phase. The broadening at the leading edge of (111) and the falling edge of (022) indicate the presence of a small amount of CuO due perhaps to dehydration of $Cu(OH)_2$. The calculated cell parameters are: $a_0 = 2.946$ Å, $b_0 = 10.544$ Å, and $c_0 = 5.238$ Å, which are in reasonable agreement with the corresponding literature values: $a_0 = 2.9471$ Å, $b_0 = 10.5930$ Å, and $c_0 = 5.2564$ Å.[17] The intensities of (111), (130), and (020) are significantly enhanced compared to the powder XRD pattern, indicating that the nanotube crystals are on average roughly perpendicular to the copper substrate with a wide distribution of tilts.

The composition inferred from the XRD pattern is consistent with the X-ray photoelectron spectrum (XPS) and the Cu

[*] Prof. S. Yang, Dr. W. Zhang, X. Wen
Department of Chemistry and Institute of Nano Science and Technology
The Hong Kong University of Science and Technology
Clear Water Bay, Kowloon, Hong Kong (China)
E-mail: chsyang@ust.hk
Prof. Z. L. Wang, Y. Berta
School of Materials Science and Engineering
Georgia Institute of Technology
Atlanta, GA 30332-0245 (USA)

[**] This work was supported by an RGC grant administered by the UGC of Hong Kong. We thank MCPF of HKUST for assistance in sample characterization.

  DOI: 10.1002/adma.200304840